Ocean Engineering 195 (2020) 106757

Contents lists available at ScienceDirect

Ocean Engineering

journal homepage: www.elsevier.com/locate/oceaneng

Deformation and fabric of soft marine clay at various cyclic load stages

Huayang Lei [a,b,*], Yinggang Xu [a], Mingjing Jiang [c], Yan Jiang [d]

[a] Department of Civil Engineering, Tianjin University, Tianjin, 300350, China
[b] Key Laboratory of Coast Civil Structure Safety of Education Ministry, Tianjin University, Tianjin, 300350, China
[c] Department of Geotechnical Engineering, College of Civil Engineering, Tongji University, Shanghai, 200092, China
[d] Terracon Consultants, Inc,2205 Rowland Ave., Savannah, GA, USA, 31404

ARTICLE INFO

Keywords:
Soft marine clay
Cyclic load
Triaxial test
Accumulated plastic strain
SEM
MIP

ABSTRACT

Soft marine clay is susceptible to deformation under cyclic loading, controlled by microstructure variations. To investigate the microscopic characteristics of soft clay with the progression of deformation under cyclic loading, a detailed study has been conducted using consolidated undrained cyclic triaxial tests, as well as mercury intrusion porosimetry (MIP) and scanning electron microscopy (SEM). The relationships between the micro parameters and accumulated plastic strain of soft marine clay are discussed. Cyclic triaxial test results show that low cyclic stress ratio (CSR) induces stable deformation, while for greater CSR the deformation of soft marine clay presents a closely linear or exponential increase, which leads to the destructuration of the soil structure. The microanalysis shows that with vibration cycles under 0.15 CSR, the content of pore obtained by SEM decreases from 37% to 25%, and large aggregates are visibly crushed into smaller ones, leading to a 24% increase in the pore numbers, which shows the slow increase of the deformation. When the CSR is greater than 0.25, large diameter pores generate resulting in divergent development of accumulated plastic strain. An empirical model of accumulated plastic strain involving micro parameter is proposed for assessing the deformation of soft marine clay.

1. Introduction

Soft marine clay is extensively distributed underground in the east coastal China and characterized with undesirable engineering properties, e.g., a high void ratio, high compressibility, high rheology, low permeability and low shear strength (Lei et al., 2016a, 2016b, 2018; Ren et al., 2018; Wang et al., 2013, 2017). In the marine environment, offshore facilities are widely constructed, e.g. suction anchors, wind turbines, gravity platforms, harbors, dockyards, lighthouse, and so on (Ren et al., 2018). These structures are suffered from vulnerable foundations with high risky serviceability, which are frequently undergoing cyclic loads, such as waves, vehicle loads, vibration of machinery, and so on (Le et al., 2018). Correspondingly settlement issues have become the primary consideration in foundation designing, construction, and monitoring. Though influencing factors of settlement issues are rationally considered, unexpected excessive settlement problems still exist (Karg and Haegeman, 2009; Yang and Feng, 2013), which needs deep research in understanding of engineering characteristics, and the response of dynamic disturbance, especially the mechanism of deformation development should be clearly studied intending to provide guidance in predicting the lifetime serviceability of offshore facilities and improve both the risk analysis and the engineering design methods.

For the mechanical behaviors of soft marine clay under cyclic loads, many scholars have conducted abundant work and have obtained many beneficial conclusions (Ansal and Erken, 1989; Werkmeister et al., 2005; Gräbe and Clayton, 2009; Li et al., 2011; Leng et al., 2017; Wang et al., 2019). Many influencing factors for the deformation of soft marine clay, e.g., waveform, vibration frequency, cyclic stress ratio, confining pressure, principal stress rotation, temperature, static deviator stress, and vibration cycle, are investigated. Cyclic stress level is demonstrated a critical factor in presenting different deformation development and the conception of critical cyclic stress ratio is established, below which the accumulated plastic strain gradually becomes stable (Hyde et al., 1993; Yang et al., 2012). Higher cyclic stress ratio over the critical value accelerates the creep behavior of soft marine clay under cyclic loading condition and produces a detrimental response of deformation characteristics (Lei et al., 2016c). Soil initial state prior to cyclic loading also exhibits peculiar responses of dynamic performance, e.g. water content, void ratio, confining pressures, degree of consolidation, and so on (Tang et al., 2014; Sun et al., 2015; Lin et al., 2017). The principal stress

* Corresponding author. School of Civil Engineering, Tianjin University, 300350, No. 135, Yaguan Road, Jinnan District, Tianjin, China.
E-mail address: leihuayang74@163.com (H. Lei).

https://doi.org/10.1016/j.oceaneng.2019.106757
Received 17 May 2018; Received in revised form 6 October 2019; Accepted 17 November 2019
Available online 6 December 2019
0029-8018/

rotation is a heated topic discussed with hollow cylindrical torsional shear tests (Gräbe and Clayton, 2009; Cai et al., 2018). Frequency is a disputed parameter for the dynamic deformation of clay soil (Lei et al., 2016a). It could be concluded the deformation of soft marine clay is a susceptible variable which has close relationships to the external factors. Under complex stratigraphic environment, the prediction and monitoring of soft marine clay foundation settlement presents large discrepancy due to limits of laboratory study. Though uncontrollable external complexity, the deformation performance are dominated by microscopic characters, which is worthy of detailed investigation (Cui and Jia, 2013; Zhang and Cui, 2017).

Currently, microscopic characteristics of soil structures are commonly assessed using scanning electron microscopy (SEM) and mercury intrusion porosimetry (MIP). SEM is a digital fractal surface scanning test which produces 2D images of interested areas. Information about particle or particle aggregates shape, size, and connections could be obtained for qualitative analysis. With the improved technologies, partial quantitative data could be calculated based on image processing software with Otsu method (Cui and Jia, 2013), but with extreme subjectivity. Fractal dimension values of the quantitatively SEM images decreased with the increasing of magnification in measured photos (Dathe et al., 2001). The image magnification was also demonstrated the effect on the relationships between size proportion and quantitative results (Liu et al., 2005). Varied grayscale value induced great differences on measured results (Bird et al., 2006). It should be noted that though SEM quantitative analysis may suffered from the operator's experience, which may not represent the precise conceptual value, quantitative work performs valuable assists on contrastive analysis. Lei et al. (2016c) conducted a series of consolidated undrained triaxial tests and verified the change in microstructure under accelerated creep conditions of soft clay. Yang et al. (2014) studied the microstructure of Hangzhou intact clay under a wave loading condition by SEM and PCAS quantitative testing technology based on fractal theory. Bock et al. (2006) investigated the micromechanical behavior of Opalinus clay and revealed the variation law of microscopic characteristics. Cuisinier et al. (2011) revealed that lime addition to clay soils changed the pore size distributions based on MIP test results.

As a summary of field research, many scholars focused much attention on solo considerations, i.e., deformation properties related to related influencing factors, microstructure studies under certain physical or mechanical states, especially for soils reaching critical state or failure. Systematic research on the microscopic variation in soft marine clay with the deformation development under cyclic loading has not been clearly assessed. Therefore, the objective of this study is to systematically investigate the change in microfeatures of soft clay subjected to cyclic loading. To achieve this, consolidated undrained cyclic tests on a batch of remolded cylinder samples were designed that terminated at different loading cycles, with a subsequent micro tests by SEM and MIP. The relationships of the microscopic parameters with engineering properties were discussed to obtain a better understanding of the development of cyclic deformation.

2. Materials and test procedure

2.1. Soil properties

The samples were obtained underground at a depth of 10–15 m from Tianjin Binhai New Area. The plastic index *Ip* is 20.6, and the natural void ratio is greater than 1.0. The hydrometer method with a TM-85° soil densimeter (Tianjin Jin'anRui Instrument Institute, China) was used to determine the grain size distribution (Fig. 1). Clay particles (diameter<0.002 mm) account for 42% of the total composition, and the remaining 58% are silt particles (0.002 mm < diameter<0.075 mm). Table 1 summarizes the physical properties of soft marine clay used in this study.

The ratio of the natural water content to the liquid limit is approximately 0.8. The liquid limit of the soil sample is 47.7%, and the plasticity index, *PI* is 27.1. It can be seen that all the data lie slightly above the A-line defined by $PI = 0.73(\omega_L - 20)$ but below the U-line defined by $PI = 0.9(\omega_L - 8)$ in the plasticity chart. Therefore, the soil sample is clay soils. According to the Unified Soil Classification System (USCS), the sample is classified as CL.

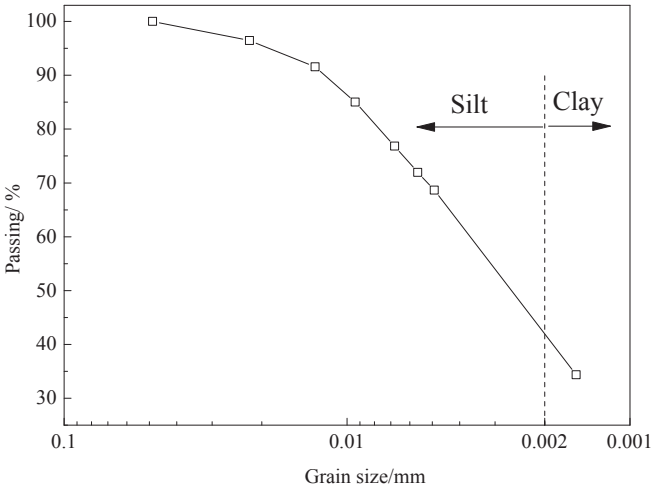

Fig. 1. Particle size distribution of soft marine clay.

Table 1
Physical and mechanical properties of the tested soil.

Characteristic index	Value
Water content, ω (%)	38
Density,ρ_0(g/cm^3)	1.91
Porosity ratio,e_0	1.14
Liquid limit,w_L(%)	47.7
Plastic limit,w_P(%)	27.1
Cohesion, c (kPa)	7.6
Internal friction angle, φ (°)	13.6
Compression index, C_c	0.3

2.2. Sample preparation

Remodeled cylindrical samples with 38.1 mm in diameter and 80 mm in height were prepared for homogeneity purpose. A batch of bulk clay was oven dried at 105–110 °C to a constant mass, allowed to cool to ambient laboratory temperature (20 °C), disaggregated, and then sieved to obtain the fraction that passes through a 2 mm sieve. The powered soil was thoroughly mixed with deionized water to obtain 40% water content, with subsequent compaction in a cylinder mold based on the natural density. The molds with the soil samples were placed into a vacuum saturator machine, where the molds were vacuumed for 2 h, and then immersed in distilled water, allowed to settle for at least 12h, which induced a good saturation level under the pressure difference.

2.3. Cyclic triaxial tests

Cyclic triaxial tests were conducted on a British GDS triaxial machine. Stress-controlled loads were applied using a digitally controlled system. Cell pressures were controlled manually with a digital transducer. Prior to the consolidation, the re-saturation of samples with back pressure was conducted and the saturability was checked using B-value method embedded in the machine system, defined as

$$B = \frac{\Delta u}{\Delta \sigma_3} \tag{1}$$

where Δu is the induced pore water pressure increment when the cell pressure increment $\Delta\sigma_3$ is applied. Once B-value is upon 97%, a series of anisotropic consolidation was carried out at a 50 kPa effective cell pressure and 100 kPa effective vertical pressure, during which drainage was permitted at the top and bottom surfaces of the sample with filter paper clinging to both ends of the sample. Once the rate of deformation was less than 0.001 mm/h or a time duration of 48 h of consolidation was reached, consolidation was terminated and followed by undrained cyclic testing. All tests were performed at the room temperature of 20 ± 2 °C. Sinusoidal waves were applied for cyclic loading, and the amplitude of the sinusoidal waves was equal to the deviatoric stress (Fig. 2). The specimens were undrained and subjected to 5000 cycles, except for those that failed (the cumulative axial strain exceeded 5%) before 5000 cycles.

In this study, the dynamic stress was considered using a parameter of the cyclic stress ratio as follows:

$$CSR = \frac{\sigma_d}{2\sigma_3^{'}} \tag{2}$$

whereσ_d is the amplitude cyclic deviator stress and $\sigma_3^{'}$ is the effective confining pressure. Four CSRs of 0.1, 0.15, 0.25, and 0.3 were considered, as shown in Table 2.

2.4. SEM analyses

Scanning electron microscopy (SEM) is a technique that produces images of a sample structure by scanning it with a focused beam of electrons. SEM has been commonly used to study the microstructures of soil samples. All samples were initially trimmed into 1 cm^3 cubes and were coated with electrically conductive material to be suitable for testing in this study (Kong et al., 1995).

Dehydrated bulk samples are required and prepared prior to the test. Freeze-drying is the most appropriate choice for dehydrating soil samples. In this study, the soil samples were rapidly frozen in liquid nitrogen (boiling point: 196 °C) for 2 min, during which water reserved within the samples sharply transformed into a solid state (amorphous ice) without enough time to recrystallize, leading to the preservation of soil structures without water volume expansion. The frozen sample was then placed in a vacuum environment at a temperature of −50 °C for at least 24 h, where the frozen moisture was sublimated and dried well. The samples under the prescribed loading conditions that needed for SEM analysis are shown in Table 2.

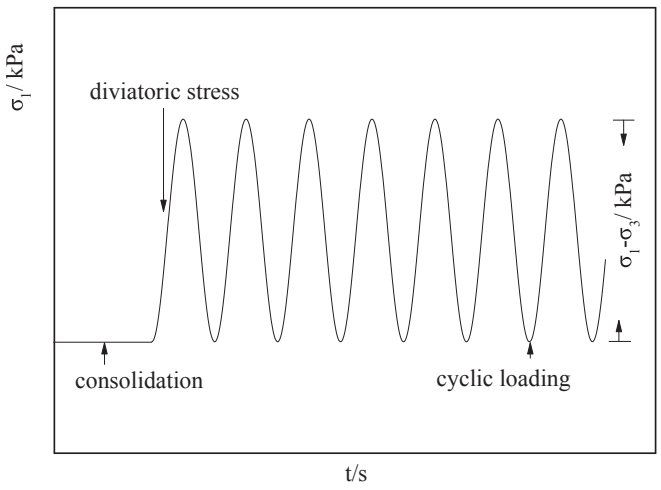

Fig. 2. Cyclic loading diagram.

Table 2
Summary of the cyclic test and microtest arrangements.

Sample ID	Effective confining pressure/kPa	Frequency/ Hz	CSR	Number of loading cycles	MIP	SEM
C1	50	–	–	0	✓	✓
C2	50	1	0.1	500	✓	
C3	50	1	0.1	1000	✓	✓
C4	50	1	0.1	3000	✓	
C5	50	1	0.1	5000		
C6	50	1	0.15	500	✓	✓
C7	50	1	0.15	1000	✓	✓
C8	50	1	0.15	3000	✓	✓
C9	50	1	0.15	5000		
C10	50	1	0.25	500	✓	
C11	50	1	0.25	1000	✓	✓
C12	50	1	0.25	3000	✓	
C13	50	1	0.25	5000	✓	
C14	50	1	0.3	200	✓	
C15	50	1	0.3	400	✓	
C16	50	1	0.3	600	✓	✓
C17	50	1	0.3	640		

2.5. MIP analyses

Mercury intrusion porosimetry (MIP) was conducted (Gallé, 2001) to verify the variations in porosity and pore size distribution. The pore size distribution curve can be obtained from the intruded volume of mercury at each pressure step. The tests were conducted in the 9510 mercury intrusion machine produced by MAC, with a measuring range of 0.003–360 μm. Prior to MIP, a freeze-drying technique similar to the SEM analysis preparation was used to remove moisture from the porous structure. MIP involves the measurement of the volume of mercury injected into the porous medium with increasing applied pressure. Pressure differences can be converted to pore diameters using the Washburn equation (Washburn, 1921).

$$p = \frac{-2\sigma\cos\alpha}{r} \tag{3}$$

where$p$is the intrusion pressure, $r$is the pore radius based on the assumption that the pores are cylindrical in shape,$\alpha$is the contact angle between mercury and soil, which remains at a constant value of 130°, and $\sigma$is a surface tension of 0.485 N/m.

During the intrusion test, the dehydrated sample was initially surrounded by mercury with a confining pressure of approximately 3 kPa. The mercury then intruded into the pores with incremental liquid pressure until the system reached its maximum capacity (406 MPa in this study). Based on the pressure-intrusion data of the test, the relationship between the pressure and the intrusion volume of the mercury was obtained, and the pore volume and its distribution were determined. The equivalent diameter could be transformed, and the pore characteristic parameters could be obtained. To investigate the microfeature variation with the deformation development, the cylinder samples that underwent triaxial cyclic loading were removed from the test apparatus and further tested by MIP. The detailed testing sets are shown in Table 2.

3. Test results

3.1. Accumulated plastic strain development

Fig. 3 shows the accumulated plastic strain variation with the number of loading cycles under different CSRs. The data demonstrates that CSR produces a significant effect on deformation development in clayed soils under cyclic loading. The accumulated plastic strain increased rapidly under initial vibration and then continued to increase in a decreasing growth rate when the CSR was 0.1 and 0.15, the accumulated plastic strain varied little after 3000 cycles and reached stable values of 1.0% and 2.4%, respectively, under which situation the

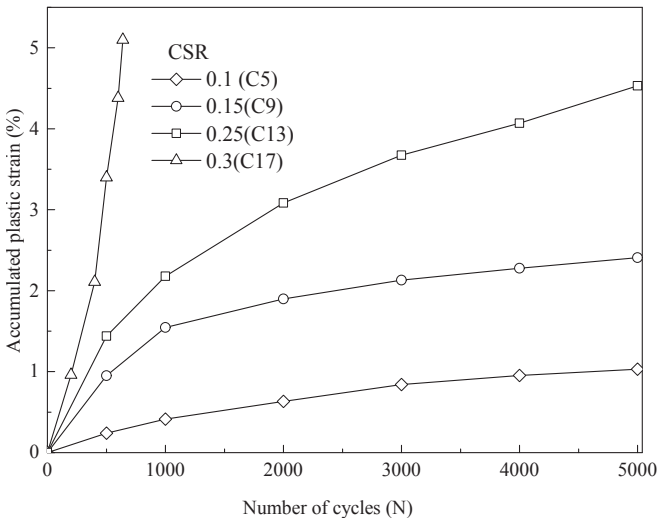

Fig. 3. Accumulated plastic strain variation with cycles under 1 Hz.

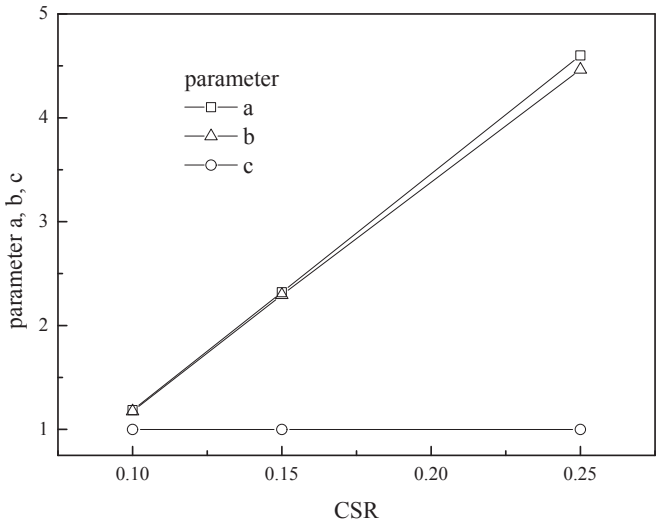

Fig. 4. a, b and c values under different CSR.

samples could not reach the failure state. When the CSR was 0.25, a decreasing rate of accumulated plastic strain growth was detected before 2000 cycles, and the accumulated plastic strain of 3.0% was recorded, which increased by 60% compared with that under a CSR of 0.15. When the cycles exceeded 2000, the accumulated plastic strain continued to increase linearly up to 4.5% when the target number of 5000 cycles was reached. It could be predicted that the samples under a CSR of 0.25 would finally fail with further loading. When CSR increased to 0.3, the accumulated plastic strain increased in exponential manner which resulted in nonconvergent development of deformation and reaching failure.

Fig. 3 demonstrates the effects of CSR on deformation progression of soft clay. When the CSR is greater than 0.2, accumulated plastic strain increases at a high rate of growth initially, and presented linear or concave grows before reaching the failure. Previous studies (Sweere, 1990; Tang et al., 2014) have reported a linear variation of accumulated plastic strain versus number of cycles plotted in double logarithmic coordinates and proposed a predictable model of the accumulated plastic strain of clays under cyclic loading as follows:

$$\varepsilon = aN^b \tag{4}$$

where$\varepsilon$is the accumulated plastic strain, N is the number of loading cycles, and a and b are measurable parameters. In this research, a model in exponential form of ε with cycles N was advised as follows:

$$\varepsilon = a - b \times c^N \tag{5}$$

where a, b, and c are undetermined parameters and the values obtained by nonlinear curve fitting mathematically were listed in Table 3.

Table 3 reveals that a, b increase with the CSR and the relationships are plotted in Fig. 4. A good linear variation was discovered and mathematical relationship a, b ~ CSR was proposed as follows:

$$a \ \ or \ \ b = 22.3 \times CSR - 1.05 \tag{6}$$

while c was almost a constant value 0.999. Based on above results, the predicted model of accumulated plastic strain,$\varepsilon$was determined as:

$$\varepsilon = (22.3 \times CSR - 1.05) \times \left(1 - 0.999^N\right) \tag{7}$$

where ε is accumulated plastic strain, CSR is cyclic stress ratio, and N is vibration cycles.

It should be pointed out that ε increase of samples under 0.3 CSR was not inconstancy with the empirical model in equation (7). The reason was that under 0.3 CSR, the deformation of soft marine clay was failure problem, so that the parameter a, b, and c are absent in Table 3. To conclude, the predicted model (Equation (7)) is valid within the limitation of power increase of ε under CSR lower than 3.0 and provide reference for settlements measurement and control for Tianjin Binhai soft clay.

Table 3
Parameters a, b, c.

CSR	a	b	c	Correlation R^2
0.1	1.186	1.175	0.9996	0.99788
0.15	2.321	2.294	0.9990	0.98839
0.25	4.600	4.465	0.9994	0.98741
0.3	–	–	–	–

3.2. Changes in the microscopic characteristics based on SEM

To clearly investigate the variation of microscopic characteristics in soft marine clay during the deformation progress subjected to cyclic loading, SEM images were captured and shown in Fig. 5. The Image-Pro

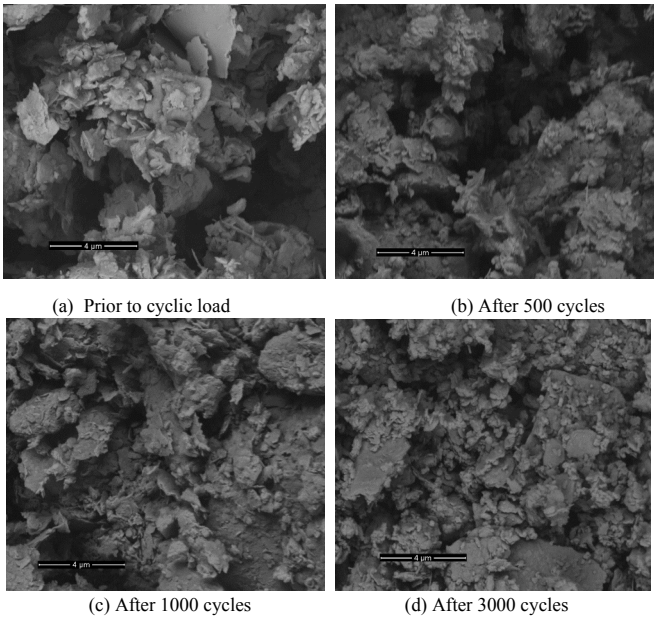

Fig. 5. SEM images of soft marine clay under continuous loading.

Plus software was used to quantify the micro-parameters summarized in Table 4. SEM images were converted to a binary 2D image with the values of 0 (white pixels) referred to soil aggregates and 1 (black pixels) referred to pores (Zhang and Cui, 2017). The grayscale value of a certain pixel between 0 and 1 was determined and a few quantitative parameters were obtained within its algorithms. Pore number is the numbers of pore counted. Pore area ratio is the percentage of pore area to the whole measured area. Max pore diameter is the longest distance calculated between two points within the pore edge. Total pore perimeter is the whole length of pore edges. Roundness is a shape parameter calculated as follows:

$$R = \frac{P^2}{4\pi S} \tag{8}$$

where R is the pore roundness; P is the pore perimeter, and S is the pore area. It could be noted that the roundness of circle is 1. Prolate shape has a roundness higher than 1.

It could be noted that in the initial micro scanning of remolded samples prior to cyclic loading, large pores were observed among the aggregates, which were formed by clay slices and occupied a large proportion of the volume composition, leading to a large pore area ratio of 37% (Table 4) for the initial state of micro-scanning. The pores are extremely internally developed, and the max pore diameter of the pores between particles is measured as 9.3 μm. The aggregates are connected through face to point and point to point contacts, which induces a significant compression potential. After 500 loading cycles, a remarkable variation is that the large pores are compressed, reducing the max pore diameter to 8.9 μm and the pore area ratio to 33%. The number of pores and the roundness varied little, demonstrating the pore shape stability. The void space decreased remarkably, leading to a sharp increase in the accumulated plastic strain. When the number of cycles increased up to 1000, the number of pores notably increased by 8%, and the total pore perimeter increased by 17% compared to that at 500 cycles, which implied that some aggregates were broken into smaller aggregates due to continuous pore compaction. The pore area ratio decreased from 33% to 23%, demonstrating an unstoppable deformation development.

It could be inferred that the growth rate of accumulated plastic strain decreased because the microstructure was densely compacted to some extent. When the number of cycles reached 3000, compared to 1000 cycles, the pore area ratio did not differ that much, while with the increase of crushed broken particles, the number of pores and the total pore perimeter slightly increased, which means that the accumulated plastic strain presented a slow growth with proceeding cyclic loading.

Fig. 6 shows the micro variation in soft marine clay under different CSRs at the same loading cycles of 1000, except for the CSR = 0.3, which failed at 600 loading cycles. It should be noted that, compared to Fig. 5, a different magnification of 10 μm was adopted to attain visible analyses of microscopic observations. The parameters of max pore diameter, pore area ratio, and roundness are independent of the observational scale variation. Table 4 shows that large pores are compressed with a pore area ratio of 36% and a max pore diameter of 8.8 μm, which resulted in the occurrence of accumulated plastic strain but without particle alteration or broken aggregates at 1000 cycles of vibration. When the CSR was 0.15, the pore area ratio reduced by 5%, which led to a larger accumulated plastic strain than that when the CSR was 0.1. Furthermore, the number of pores sharply increased by 56%, which implied that some large diameter aggregates were broken into smaller aggregates.

In contrast, for 0.25 CSR, compaction continued to occur and the pore area ratio reduced to 28%. However, the max pore diameter was measured at 18 μm, twice as much as that for CSR 0.15. The data revealed that large shear deformation was produced, which induced an unstable increase in accumulated plastic strain. When the CSR was 0.3, the pore area ratio was measured at 43%, and the max pore diameter was 29 μm. The roundness was strikingly calculated as 151, which demonstrated the overall irregular shape of the pores. This fact implied that a large amount of deformation developed and was not convergent. The statistics revealed the influence of the CSR on micro variations controlling the deformation development. A low CSR, e.g., 0.1 or 0.15, would lead to a stable compaction of void spaces, particle size arrangement, and thus steady deformation progression. For a high CSR, 0.25 and 0.3, the particles were compacted and large pores were regenerated, inducing divergent accumulated plastic strain.

3.3. Pore size distribution of MIP data

The pore diameter classification of soil provides remarkable convenience for analyzing micropore features and has been reported by many scholars. Lei (1985) conducted a mercury intrusion test on the loess in Xi'an and classified the pore diameters as extra-large pores (>250 μm), large pores (250-16 μm), medium-size pores (16-4 μm), small pores (4-1 μm) and micropores (<1 μm). Based on the statistical self-similarity principle method, Jiang et al. (2010) put forward the pore division segments of typical silt clays in Tianjin after dynamic loading: large pores (>0.8 μm), medium-size pores (0.8–0.01 μm), and micro pores (<0.01 μm). According to the mercury intrusion test data in this study, the pore size in this study is classified into the following categories: extra-large pores (>3 μm), large pores (3-1 μm), medium-size pores (1–0.1 μm), small pores (0.1–0.01 μm) and micro pores (<0.01 μm).

The pore size distribution of the soft marine clay subjected to cyclic loading with varied CSR and loading cycles are summarized in Table 5. Pore size variation in dependent of incremental cycles was analyzed when CSR was 0.25. The pore diameters of samples without cyclic loading are mainly distributed in the range of 0.01–3 μm, with the volume percentages of small, medium-size, and large pores being 17.2%, 41.7%, and 33.3%, respectively. When CSR was 0.25, after 500 loading cycles, the medium-size pore and small pore contents increased considerably 17.4% and 2.8% compared with the sample not subjected to cyclic loading, while the large pore content decreased 18.9%, which implies that the initial sharp increase of accumulated plastic strain is a result of large pore compaction. With continuous loading cycles increased up to 1000, the medium-size pore content reduced 2.4% compared to 500 cycles. This indicates that the structure is kept compacted and the slowing deformation could be predicted. The small pore content increased 3.2%, which also demonstrated the slow increase of deformation.

After vibration cycles 3000, the small and medium-size pore contents continues to decrease while large and extra-large pore contents shows the tendency of increase, implying that deformation continues to

Table 4
Summary of microscopic characteristic parameters.

Conditions	Variations	Pore Num.	Pore area ratio	Max pore diameter/μm	Roundness	Total pore perimeter/μm
f = 1 Hz, CSR = 0.15	0	1029	37%	9.3	2.8	359
	500 cycles	1050	33%	8.9	2.9	394
	1000 cycles	1129	23%	7.4	3.2	461
	3000 cycles	1272	25%	7.5	3	483
f = 1 Hz, Cycles = 1000	CSR = 0.1	2514	36%	8.8	2.9	2439
	CSR = 0.15	3933	31%	7.7	3.4	4187
	CSR = 0.25	4020	28%	18	4	4223
	CSR = 0.3	1353	43%	29	151	2661

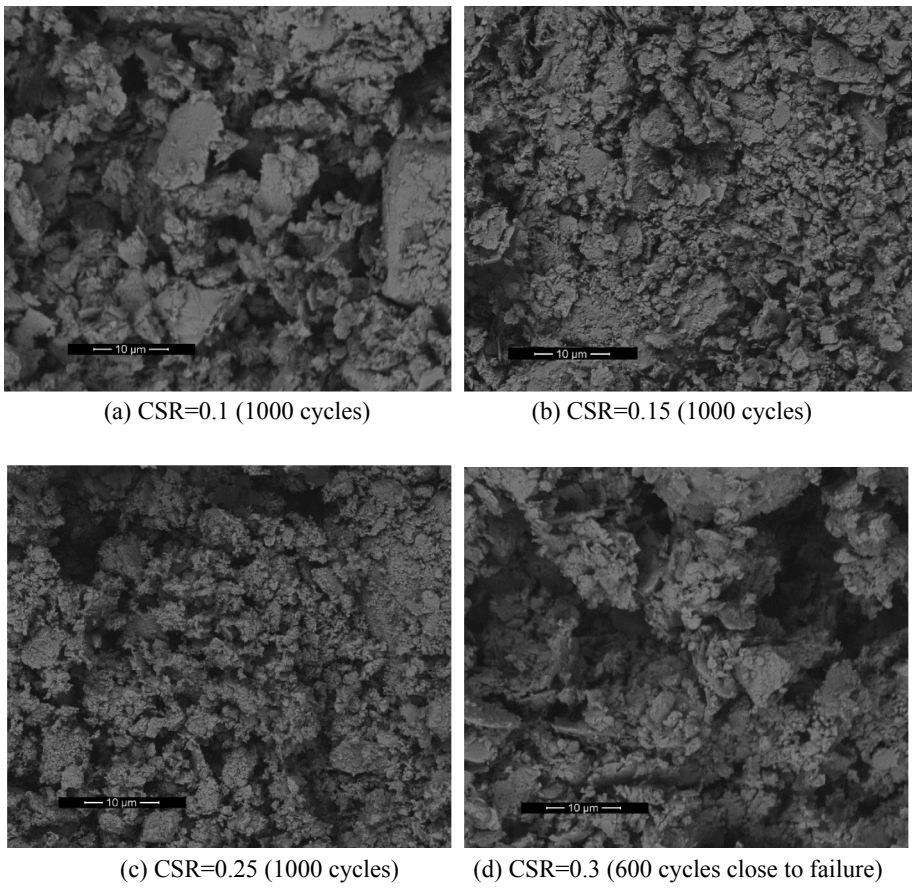

(a) CSR=0.1 (1000 cycles) (b) CSR=0.15 (1000 cycles)

(c) CSR=0.25 (1000 cycles) (d) CSR=0.3 (600 cycles close to failure)

Fig. 6. SEM images of soft clay under different CSR.

Table 5
Pore size distribution of samples under different CSRs and cycles.

CSR	Cycles	Pore size distribution/%				
		micro pore	small pore	medium-size pore	large pore	extra-large pore
		/μm	/μm	/μm	/μm	/μm
		<0.01	0.01–0.1	0.1–1	1–3	>3
0	0	0.6	17.2	41.7	33.3	7.2
0.1	500	3.7	23.5	51.1	17.4	4.3
	1000	3.9	25	53.4	12.9	4.8
	3000	2.8	35.3	46.1	14.4	1.4
0.15	500	4.2	22.3	55.6	13.8	4.1
	1000	2.1	24.7	57.6	13.4	2.2
	3000	3.7	30.4	48.3	15.7	1.9
0.25	500	2	20	59.1	14.4	4.5
	1000	1.9	23.2	56.7	12.6	5.6
	3000	1.7	22.1	48.3	18.2	9.7
	5000	2.1	19.4	45.1	24.1	9.3
0.3	200	4	34.1	48.4	10.4	3.1
	400	2.3	23.7	51.3	18.6	4.1
	600	1.8	16.3	49.4	20.1	12.4

develop. When loading cycles reaches 5000 under 0.25 CSR, large pore content was 24.1%, increased 5.9% compared to that in 3000 loading cycles. The increasing tendency in large pore content implies the continuously increase of accumulated plastic strain under higher vibration cycles, under which situation, the soil structure has become unstable, with a predictable failure state with afterward continuous loading.

The variations of pore size distribution among different CSRs were compared with the same loading cycle. When the number of cycles is lower than 1000, the pore content under each classification slightly changed with CSR varied from 0.1 to 0.25. This implied that under a small number of cycles, the effect of the CSR was not remarkable for the deformation occurred at early vibration much due to large pore compression. When the cycles reach 3000, a remarkable variation in extra-large pore content under 0.25 CSR was observed as 9.7%, while under 0.1 and 0.15 CSR, it was just 1.4% and 1.9%. This indicates that extra-large pore occurrence has offered the predictability of unstable deformation development. Analogous phenomenon was also observed when samples cyclic loaded up to fail under 0.3 CSR, with astonishing extra-large pore content, 12.4%. The MIP data analyses shows the inconsistency with the SEM results and deformation progression.

4. Relationship between the microscopic characteristics and engineering properties

Mechanical behaviors, by their very nature, are dominated by the microscopic characteristics, and many scholars tried to reveal the macro responses from the perspective of micro-investigation. Chang et al. (2009) assumed that clay material can be considered as assemble of clusters. The deformation is generated by the mobilizing and compressing of all clusters (Yin et al., 2011; Yin and Hicher, 2013). Microstructure modelling is established and verified related to shearing behaviors (Yin and Chang, 2009; Yin et al., 2009) and cyclic behaviors (Yin et al., 2012). For clear insight of the deformation development, micro parameter corresponding to the accumulated plastic strain is investigated.

Fig. 7 shows the variation of specific surface area with vibration cycles, corresponding to the accumulated plastic strain. The evolution of deformation could be summarized into three stages: stage I, initial compression. In Stage I (initial compression stage), the sharp increase of

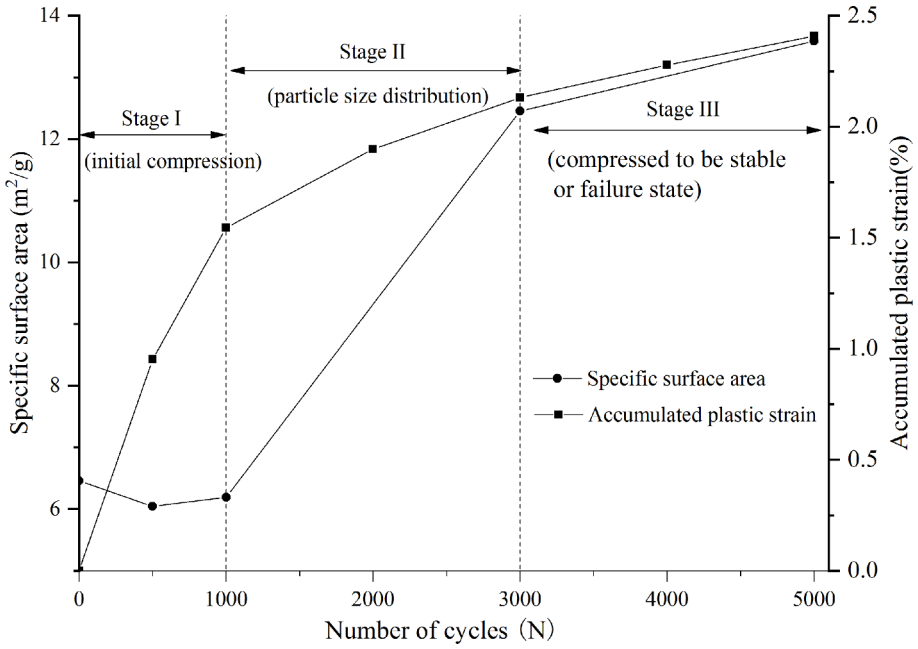

Fig. 7. Variation of specific surface area with vibration cycles.

accumulated plastic strain is much deduced from the (extra) large pores compression. It could be demonstrated that the specific surface area is almost unchanged, which implies that the particle shape is relatively unchanged. The particle number is around 1050. In Stage II (particle size distribution stage), the deformation continuously increases as the result of broken aggregates. The specific surface area doubles which demonstrates the smaller diameter particles are generated, and the particle number increases to around 1300. In Stage III (stable stage or failure state), the specific surface area slightly increases to a stable value which may show the continual compaction.

As the deformation of soft clay is mainly caused by the change in pore size (compression), which is closely related to the size and size distribution of soil particles, based on the mercury intrusion test data, median pore diameter was selected for correlation analysis, below (above) which the cumulative pore volume occupies 50% of the total void space.

Fig. 8 shows the variation in the median pore diameter with the number of loading cycles for the samples subjected to cyclic loading (CSR = 0.15, frequency = 1 Hz). It can be seen that the median pore diameter decreases inversely with the vibration cycles overall. Detailed observation reveals that at early-stage vibration, the median pore diameter linearly decreases by 20% from 0.78 to 0.62 μm, which reveals a fast increase in deformation. When the number of cycles exceeds 1000, the median pore diameter decreases slowly to 0.54 μm at 3000 cycles and 0.52 μm at 5000 cycles, which tends to become constant value. The median pore diameter reflects the degree of void compaction and indirectly reveals the particle size distribution, which is in good agreement with the deformation progress; therefore, it may be useful for predicting the accumulated plastic strain for samples, with the advantage of convenience in physical index testing while ignoring external complex factors. Based on this consideration, an empirical model of the median pore diameter versus the number of cycles is proposed as follows:

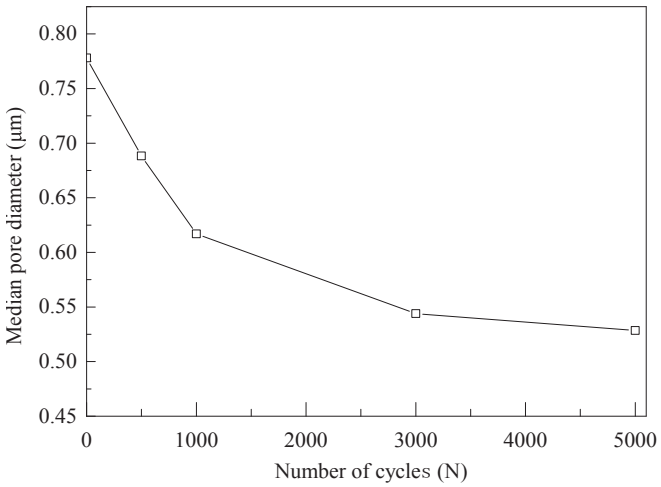

Fig. 8. Variation in the median pore diameter with the number of cycles.

$$D = 0.53 + 0.25 \times 0.999^{N} \tag{9}$$

where D is the median pore diameter (μm) and N is the number of vibration cycles. The relationship between accumulated plastic strain and the number of vibration cycles has been revealed in formula (7). Thus, the predicted model of accumulated plastic strain related to the median pore diameter can be obtained via mathematical conversion:

$$\varepsilon = (0.78 - D) \times (89.2 \times CSR - 4.2) \tag{10}$$

where D is the median pore diameter (μm) and ε is the accumulated plastic strain (%). It should be noted that this prediction model is based on Eq. (7), with a same validity limitation of lower CSR than 0.3, powerful increase of ε for Tianjin Binhai soft clay. It can be discussed that CSRs lower than 0.25 leads to stable deformation. High CSR values increase the risk of failure and should be avoided and fully considered in the design of a project in practice.

Fig. 9 shows the three dimensional variation of accumulated plastic strain of samples in medium pore diameter-CSR space. It can be seen that the accumulated plastic strain was settled in a nonlinear 3D surface and lower CSR and high medium pore diameter induced a small accumulated plastic strain. With the variation of medium pore diameter, striking change could be observed in ε which showed the close relation between these two measurements and the validity of representative of ε using medium pore diameter D.

Fig. 10 shows the variation of median pore diameter with accumulated plastic strain of samples under different CSRs. It can be seen that

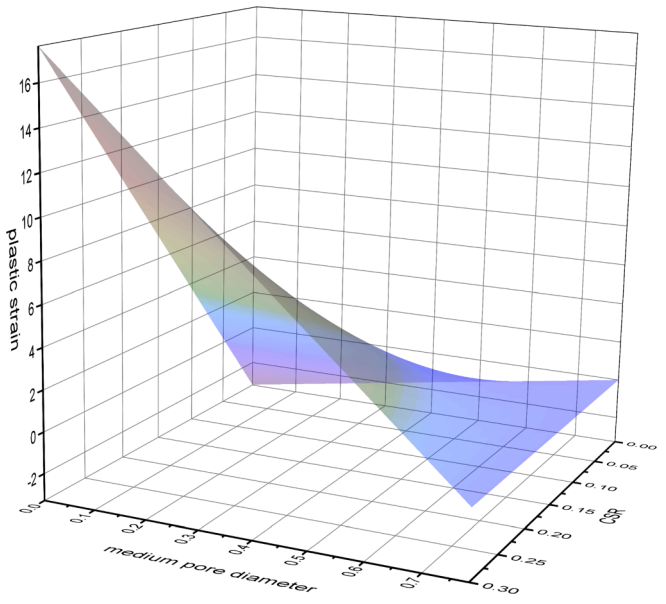

Fig. 9. 3D surface of accumulated plastic strain in D-CSR space.

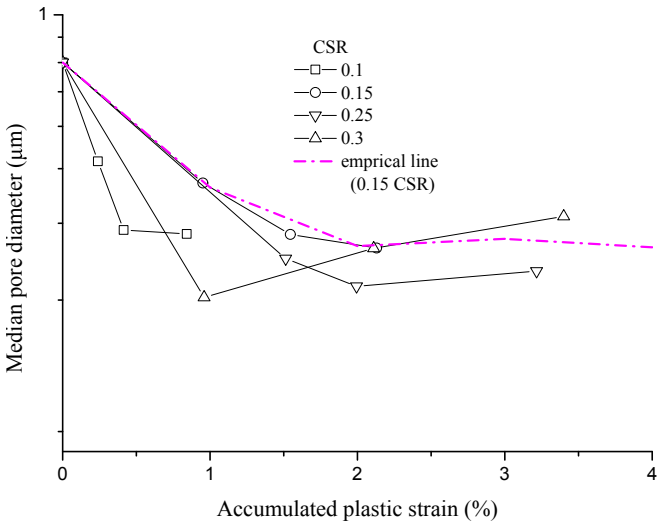

Fig. 10. Variation of median pore diameter with plastic strain.

the median pore diameter reduces with the plastic strain increases from a whole view. When CSR is 0.1, a linear reduction of median pore diameter is observed in the prophase variation, but tends to become a constant at the final phase. Furthermore, under the same vibration cycles, the stable plastic strain under CSR is about 1%, far less than other CSRs. The variation character of median pore diameter shows a favorable agreement with the deformation development. When CSR is 0.15, the curve trend is similar to the variation of 0.1 CSR, with the difference showing that much further deformation progress is observed under 0.15 CSR. Median pore diameter decreases by 60% during cyclic loading under 0.15 CSR. When CSR is 0.25 or 0.3, a notable point different from smaller CSRs is that median pore diameter rises in later cyclic load phases rather than becomes stable. The likely reason is that under these CSRs, deformation of samples is not convergent, which leads to the severe failure of soil structure, thus generating new large pores, increasing the median pore diameter. It should be noted that the empirical model is displayed in colored dot lines in Fig. 10. It can be seen that the empirical line is in good consistency with the test line, which demonstrates the reliability of the proposed model for practice probability.

Fig. 11 shows the variation in the median pore diameter with CSR under different vibration cycles. An overall reduction in the median pore diameter is observed. A linear reduction of median pore diameter with CSR increase was observed. Additionally, the data point in 0.3 CSR was far deviated from the linear trace. The reason was that predictable model was valid with its own limitations: CSR lower than 0.3, powerful increase of ε. This point may be exactly a demonstration of the model accuracy.

5. Conclusions

Laboratory work was conducted to investigate the deformation progress of soft marine clay under cyclic loading, and scanning electron microscopy (SEM) and mercury intrusion porosimetry (MIP) tests were carried out to reveal the microfeature variations. Correlation analyses between the microscopic characteristics and the deformation progress were performed to strengthen the understanding of the dynamic deformation of soft marine clay. The following conclusions were drawn:

(1) The cyclic stress ratio (CSR) produced a pronounced effect on the deformation properties of soft clay. High CSRs than 0.25 induced failure accumulated plastic strains. For low CSRs such as 0.1 or 0.15, the deformation increased gradually to a constant value, while for CSRs greater than 0.2, the deformation of soft clay presented a linear or power increase, which led to the destruction of the soil structure. A predictable model of accumulated plastic strain related to cycles was proposed for evaluation of deformation development.

(2) Large pores with extreme internal widths and depths among the aggregates of clay slices were observed in samples prior to cyclic loading based on SEM images. Under initial vibration, the large pores were strongly compressed, resulting in a sharp increase in accumulated plastic strain. With increasing vibration cycles, the pore area ratio obtained by SEM decreased from 37% to 25%, and the large aggregates were visibly crushed into smaller aggregates, leading to a 24% increase in the number of pores, which led to the slowly increase of deformation under low CSRs. When CSR was higher than 0.25, large diameter pores were regenerated at later-stage load, resulting in divergent development of accumulated plastic strain. The MIP data showed that the content of pores in 1–3 μm diameter decreased by approximately 20%, while the pores in 0.01–1 μm diameter increased by approximately 15%, which indicates void compression behavior and accumulated plastic strain occurrence at early-stage vibration. With increasing cycles, the pore size distribution tended to be stable under low

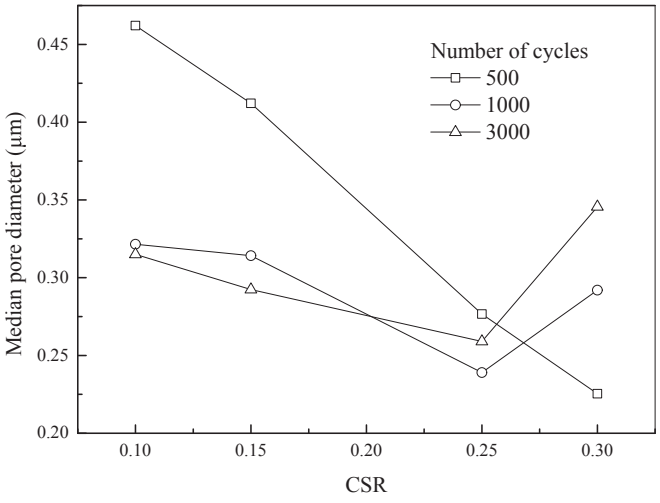

Fig. 11. Variation in the median pore diameter with CSR.

CSRs, while for high CSRs, the large pore content showed a tendency to increase, resulting from the continuous progression of deformation.

(3) The median pore diameter decreased with increasing cycles. The empirical model of accumulated plastic strain related to median pore diameter and CSR was established for assessing the strain state in subgrade settlement monitoring, taking advantage of indoor soil physical testing. Noted that the proposed model should be valid for CSRs lower than 0.3, accumulated plastic strain in exponential increase in Tianjin Binhai soft clay.

Acknowledgements

The authors are grateful to the National Key Research and Development Program of China (Grant No. 2017YFC0805402), the Program of National Natural Science Foundation of China (Grant No. 51578371), Open Project of State Key Laboratory of Disaster Reduction in Civil Engineering, Shanghai, China (Grant No. SLDRCE17-01) and the National Science Foundation of Tianjin (Beijing-Tianjin-Hebei Special Projects) (Grant No. 16JCJDJC40000) for funding this work.

References

Ansal, A.M., Erken, A., 1989. Undrained behavior of clay under cyclic shear stresses. J. Geotech. Eng. 115 (7), 968–983.
Bird, N., Díaz, M.C., Saa, A., Tarquis, A.M., 2006. Fractal and multifractal analysis of pore-scale images of soil. J. Hydrol 322 (1–4), 211–219.
Bock, H., Blümling, P., Konietzky, H., 2006. Study of the micro-mechanical behaviour of the opalinus clay: an example of co-operation across the ground engineering disciplines. Bull. Eng. Geol. Environ. 65 (2), 195–207.
Cai, Y., Wu, T., Guo, L., Wang, J., 2018. Stiffness degradation and plastic strain accumulation of clay under cyclic load with principal stress rotation and deviatoric stress variation. J. Geotech. Geoenviron. Eng. 144 (5), 04018021.
Chang, C.S., Hicher, P.Y., Yin, Z.Y., Kong, L.R., 2009. Elastoplastic model for clay with microstructural consideration. J. Eng. Mech. 135 (9), 917–931.
Cui, Z.D., Jia, Y.J., 2013. Analysis of electron microscope images of soil pore structure for the study of land subsidence in centrifuge model tests of high-rise building groups. Eng. Geol. 164 (12), 107–116.
Cuisinier, O., Auriol, J.C., Borgne, T.L., Deneele, D., 2011. Microstructure and hydraulic conductivity of a compacted lime-treated soil. Eng. Geol. 123 (3), 187–193.
Dathe, A., Eins, S., Niemeyer, J., Gerold, G., 2001. The surface fractal dimension of the soil–pore interface as measured by image analysis. Geoderma 103 (1–2), 203–229.
Gallé, C., 2001. Effect of drying on cement-based materials pore structure as identified by mercury intrusion porosimetry: a comparative study between oven-, vacuum-, and freeze-drying. Cement Concr. Res. 31 (10), 1467–1477.
Gräbe, P.J., Clayton, C.R., 2009. Effects of principal stress rotation on permanent deformation in rail track foundations. J. Geotech. Geoenviron. Eng. 140 (2), 23–42.
Hyde, A.F.L., Yasuhara, K., Hirao, K., 1993. Stability criteria for marine clay under one-way cyclic loading. J. Geotech. Eng. 119 (11), 1771–1789.
Jiang, Y., Lei, H.Y., Zheng, G., Yang, X.J., 2010. Fractal study of microstructure variation of structured clays under dynamic loading. Rock Soil Mech. 31 (10), 3075–3080.
Karg, C., Haegeman, W., 2009. Elasto-plastic long-term behavior of granular soils: experimental investigation. Soil Dyn. Earthq. Eng. 29 (1), 155–172.
Kong, L.W., Luo, H.X., Tan, L.R., 1995. Fractal study on pore space distribution of red clay in China. In: Proc. 10th ARC- SMFE, Beijing, China, vol. 1, pp. 139–142.
Le, C.H., Lee, S.H., Vicent, S., Kim, S.R., 2018. An experimental investigation of the cyclic response of bucket foundations in soft clay under one-way cyclic horizontal loads. Appl. Ocean Res. 71, 59–68.
Lei, H.Y., Xu, Y.G., Li, X., Zheng, G., Liu, G.X., 2018. Effects of polyacrylamide on the consolidation behavior of dredged clay. J. Mater. Civ. Eng. 30 (3), 04018022, 2018.
Lei, H., Li, B., Lu, H., Ren, Q., 2016. Dynamic deformation behavior and cyclic degradation of ultrasoft soil under cyclic loading. J. Mater. Civ. Eng. 28 (11), 04016135.
Lei, H., Liu, J., Liu, M., Zhang, Z., Jiang, M., 2016. Effects of frequency and cyclic stress ratio on creep behavior of clay under cyclic loading. Mar. Geotechnol. 35 (2), 281–291.
Lei, H., Lu, H., Wang, X., Ren, Q., Li, B., 2016. Changes in soil micro-structure for natural soft clay under accelerated creep condition. Mar. Geotechnol. 34 (4), 365–375.
Lei, X.Y., 1985. Characteristics of loess pore distribution in north shanxi and east gansu. Chin. Sci. Bull. 30 (5), 656–661.
Leng, J., Ye, G.L., Ye, B., Jeng, D.S., 2017. Laboratory test and empirical model for shear modulus degradation of soft marine clays. Ocean Eng. 146, 101–114.
Li, L.L., Dan, H.B., Wang, L.Z., 2011. Undrained behavior of natural marine clay under cyclic loading. Ocean Eng. 38 (16), 1792–1805.
Lin, B., Zhang, F., Feng, D., Tang, K., Feng, X., 2017. Accumulative plastic strain of thawed saturated clay under long-term cyclic loading. Eng. Geol. 231, 230–237.
Liu, Z.B., Shi, B., Inyang, H.I., Cai, Y., 2005. Magnification effects on the interpretation of sem images of expansive soils. Eng. Geol. 78 (1–2), 89–94.
Ren, X.W., Xu, Q., Teng, J., Zhao, N., Lv, L., 2018. A novel model for the cumulative plastic strain of soft marine clay under long-term low cyclic loads. Ocean Eng. 149, 194–204.
Sun, L., Gu, C., Wang, P., 2015. Effects of cyclic confining pressure on the deformation characteristics of natural soft clay. Soil Dyn. Earthq. Eng. 78 (9), 99–109.
Sweere, G.T.H., 1990. Unbound Granular Bases for Roads. PhD Thesis. Delft University of Technology, Delft, the Netherlands.
Tang, Y., Li, J., Wan, P., Yang, P., 2014. Resilient and plastic strain behavior of freezing–thawing mucky clay under subway loading in shanghai. Nat. Hazards 72 (2), 771–787.
Wang, J., Guo, L., Cai, Y.Q., Bian, X.C., Gu, C., 2013. Strain and pore pressure development on soft marine clay in triaxial tests with a large number of cycles. Ocean Eng. 74, 125–132.
Wang, Y., Gao, Y., Guo, L., Cai, Y., Li, B., Qiu, Y., Mahfouz, A.H., 2017. Cyclic response of natural soft marine clay under principal stress rotation as induced by wave loads. Ocean Eng. 129, 191–202.
Wang, Y., Lei, J., Wang, Y., 2019. A post-cyclic strength degradation model for saturated soft clay. Ocean Eng. 186, 106072.
Washburn, E.W., 1921. Note on the method of determining the distribution of pore sizes in a porous material. Proc. Natl. Acad. Sci. U.S.A. 7, 115–116.
Werkmeister, S., Dawson, A.R., Wellner, F., 2005. Permanent deformation behaviour of granular materials. Road Mater. Pavement Des. 6 (1), 31–51.
Yang, C., Jian, Z., Yan, J.J., 2014. Study of microstructures of soft clay under dynamic loading considering effect of cyclic stress ratio and frequency. Rock Soil Mech. 35 (3), 735–743.
Yang, G., Yang, Q., Liu, W., Zhang, K., 2012. Critical cyclic stress ratio of reconstituted silty clay under the cyclic loading. J. Convers. Info Technol. 7 (23), 1–8.
Yang, J., Feng, Q.B., 2013. A new method for measuring subgrade settlement in high-speed railway by using a linear ccd. Measurement 46 (5), 1751–1756.
Yin, Z.Y., Chang, C.S., 2009. Microstructural modelling of stress-dependent behaviour of clay. Int. J. Solids Struct. 46 (6), 1373–1388.
Yin, Z.Y., Chang, C.S., Hicher, P.Y., Karstunen, M., 2009. Micromechanical analysis of kinematic hardening in natural clay. Int. J. Plast. 25 (8), 1413–1435.
Yin, Z.Y., Hattab, M., Hicher, P.Y., 2011. Multiscale modeling of a sensitive marine clay. Int. J. Numer. Anal. Methods Geomech. 35 (15), 1682–1702.
Yin, Z.Y., Xu, Q., Chang, C.S., 2012. Modeling cyclic behavior of clay by micromechanical approach. J. Eng. Mech. 139 (9), 1305–1309.
Yin, Z., Hicher, P.Y., 2013. Micromechanics-based model for cement-treated clays. Theor. Appl. Mech. Lett. 3 (2), 021006.
Zhang, Z.L., Cui, Z.D., 2017. Analysis of microscopic pore structures of the silty clay before and after freezing–thawing under the subway vibration loading. Environ. Earth Sci. 76 (15), 528.